Comparison of the Fermi-surface topologies of κ-$(BEDT\text{-}TTF)_2Cu(NCS)_2$ and its deuterated analogue

2003 J. Phys.: Condens. Matter 15 L483

(http://iopscience.iop.org/0953-8984/15/31/101)

INSTITUTE OF PHYSICS PUBLISHING JOURNAL OF PHYSICS: CONDENSED MATTER

J. Phys.: Condens. Matter **15** (2003) L483–L490 PII: S0953-8984(03)61325-1

LETTER TO THE EDITOR

Comparison of the Fermi-surface topologies of κ-(BEDT-TTF)$_2$Cu(NCS)$_2$ and its deuterated analogue

R S Edwards[1], A Narduzzo[1], J Singleton[1,2], A Ardavan[1] and J A Schlueter[3]

[1] Oxford University Department of Physics, Clarendon Laboratory, Parks Road, Oxford OX1 3PU, UK
[2] National High Magnetic Field Laboratory, Los Alamos National Laboratory, TA-35, MS-E536, Los Alamos, NM 87545, USA
[3] Materials Science Division, Argonne National Laboratory, Argonne, IL 60439, USA

E-mail: jsingle@potsi.lanl.gov

Received 21 March 2003
Published 23 July 2003
Online at stacks.iop.org/JPhysCM/15/L483

Abstract

We have measured details of the quasi-one-dimensional (Q1D) Fermi-surface sections in the organic superconductor κ-(BEDT-TTF)$_2$Cu(NCS)$_2$ and its deuterated analogue using angle-dependent millimetre-wave techniques. There are differences in the corrugations of the Fermi surfaces in the deuterated and undeuterated salts. We suggest that this is important in understanding how deuteration affects the superconducting transition temperature. The data suggest that the 'nestability' of the Q1D Fermi sheets may be important in understanding the 'universal' phase diagram of κ-(BEDT-TTF)$_2$X, in agreement with other recent studies. The experiments also support models for superconductivity which invoke electron–electron interactions depending on the topological properties of the Fermi surface.

(Some figures in this article are in colour only in the electronic version)

The phase diagram of the quasi-two-dimensional (Q2D) organic (super)conductors κ-(BEDT-TTF)$_2$X, where X is Cu[N(CN)$_2$]Cl, Cu[N(CN)$_2$]Br or Cu(NCS)$_2$ (figure 1), has attracted considerable attention [1–8]. These materials possess simple Fermi surfaces (FSs) consisting of a closed pocket and a pair of quasi-one-dimensional (Q1D) sheets (figure 1 inset) [9]. Recent experiments have indicated that the tendency of the Q1D sheets to nest, causing density waves and/or antiferromagnetic fluctuations, may be of great importance. First, the antiferromagnetic insulator (AFI) state of κ-(BEDT-TTF)$_2$Cu[N(CN)$_2$]Cl [2] may have more of the character of a spin-density-wave (SDW) [3] than a Mott insulator.

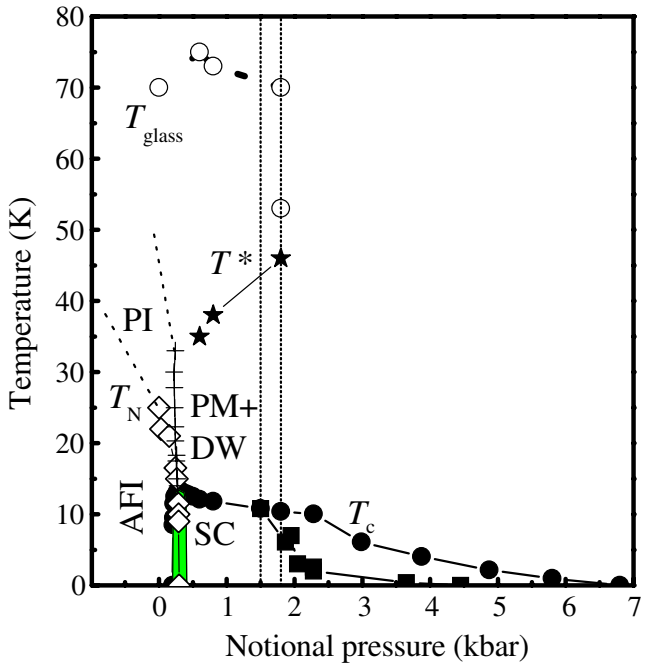

Figure 1. Phase diagram of κ-(BEDT-TTF)$_2$X, including boundaries suggested by recent data [8]. AFI = antiferromagnetic insulator below T_N (◇) [2]; PI = paramagnetic insulator [2]; PM = paramagnetic metal; DW = proposed density wave below T^* (★) [4]; SC = superconductivity below T_c (●) [5]; T_{glass}(○) = proposed glassy structural transition [3]. 'Notional pressure' combines chemical pressure caused by changing anion X [3, 4] and applied hydrostatic pressure [5]; '0' is ambient pressure for κ-(BEDT-TTF)$_2$Cu[N(CN)$_2$]Cl; the vertical lines are the ambient pressure positions of d8 (left) and h8 (right) κ-(BEDT-TTF)$_2$Cu(NCS)$_2$. Note that it has been proposed that T_c has a different pressure dependence for h8 and d8 [5]; to make this distinction, T_c points for d8 are shown as filled squares. The inset shows the FS cross-section of κ-(BEDT-TTF)$_2$X [9].

Second, recent data suggest the existence of a charge-density-wave (CDW)-like state coexisting with the metallic state that is the precursor to superconductivity [4]. Finally, experiments supporting an order parameter exhibiting nodes (see [6, 10] and references therein), plus the proximity of superconductivity to the AFI [1, 2, 7] have led to theoretical treatments that invoke superconducting pairing mediated by electron–electron interactions and/or antiferromagnetic fluctuations [11, 12]. In such a scenario, the 'nestability' of the FS is again an important consideration; small changes in topology should produce significant changes in superconducting transition temperature T_c.

In this letter we describe millimetre-wave measurements which compare the Q1D FS sections of conventional κ-(BEDT-TTF)$_2$Cu(NCS)$_2$ (referred to as h8) with those of samples in which the terminal hydrogens of the BEDT-TTF molecules have been replaced with deuterium (referred to as d8) [13]. Based on the consequent increase in T_c for κ-(BEDT-TTF)$_2$Cu(NCS)$_2$ [5, 13] and enhanced antiferromagnetic behaviour in κ-(BEDT-TTF)$_2$Cu[N(CN)$_2$]Br [4, 7], deuteration is said to be equivalent to a shift to the left on the 'pressure' axis of figure 1. Our data suggest that it is changes in the topology of the FS that cause this shift, illustrating the importance of the Q1D FS section [3, 4] and supporting models for superconductivity involving pairing via electron–electron interactions [11, 12].

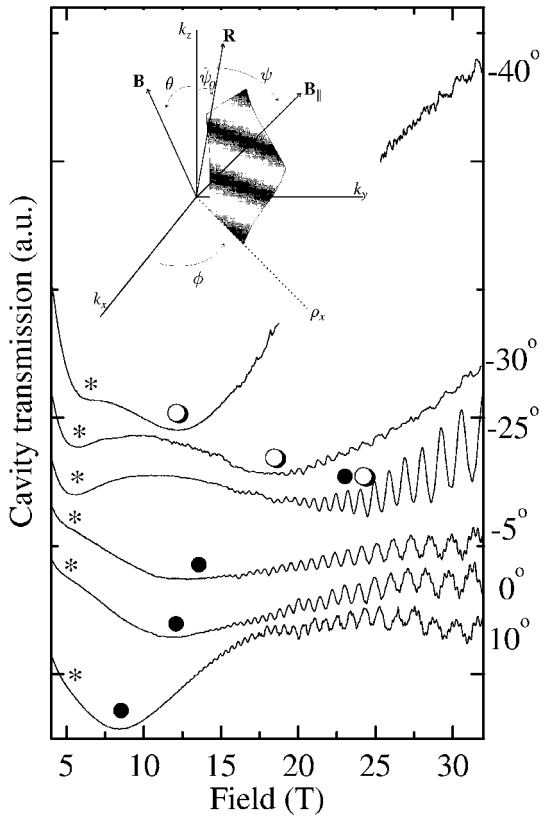

Figure 2. Transmission of a cavity loaded with a d8 sample versus field ($T = 1.5$ K, $\phi = 5°$) for several θ angles (shown on right). Data are normalized and offset for clarity; $*$ shows the position of the feature close to $\mu_0 H_{c2}$; ○ and ● show the FTRs. Inset: the relationship between the coordinates $\boldsymbol{B}$, θ and ϕ, the field component $\boldsymbol{B}_\parallel$ and the angles ψ and ψ_0. $\boldsymbol{R}$ indicates the axis of the FS corrugation; the FS lies in the plane defined by ρ_x. In κ-(BEDT-TTF)$_2$Cu(NCS)$_2$, k_x, k_y lie in the $\boldsymbol{b}$, $\boldsymbol{c}$ plane; k_z is parallel to $\boldsymbol{a}^*$.

FS traversal resonances (FTRs) [14] (resonances in the high-frequency conductivity caused by magnetic-field-induced motion of quasi-particles across the Q1D sheets) are used to infer the corrugations of the sheets. The experiments involved single crystals of h8 and d8 ($\sim 0.7 \times 0.5 \times 0.1$ mm^3; mosaic spread $\lesssim 0.1°$), produced using electrocrystallization [13]. A single sample is mounted at the centre (in a magnetic field antinode) of a rectangular cavity of inner dimensions $1.55 \times 3.10 \times 6.00$ mm^3 resonating at 72 GHz in the TE$_{102}$ mode [14]; the oscillating H-field lies within the sample's Q2D ($\boldsymbol{b}$, $\boldsymbol{c}$) planes. In this configuration, the effective skin depth is very large, and the gigahertz fields penetrate the bulk of the sample [15, 16]. The cavity can be rotated with respect to the external quasi-static magnetic field $\boldsymbol{B}$ so as to vary the angle θ between $\boldsymbol{B}$ and the normal to the sample's Q2D planes [14]; the normal to the Q2D planes is the $\boldsymbol{a}^*$ direction of the reciprocal lattice [17, 18]. In addition, the sample can be turned about $\boldsymbol{a}^*$ within the cavity, so as to vary the plane of rotation, defined by the azimuthal angle ϕ [14]. The angles θ and ϕ and their relationship to the Q1D sheet of the FS are given in the inset to figure 2; $\phi = 90°$ corresponds to rotating in the $\boldsymbol{a}^*$, $\boldsymbol{b}$ plane.

Experiments were carried out on two different samples of d8; all gave consistent results. This paper deals with the sample with the most complete data set, covering angles

Table 1. The values for A/ω (see equation (1)), ψ_0 (angle of corrugation axis with respect to $\boldsymbol{a}^*$) and Ψ_0 (angle of corrugation axis with respect to $\boldsymbol{a}$) for each of the FTRs seen in d8 and h8 κ-(BEDT-TTF)$_2$Cu(NCS)$_2$. Also shown are the vectors $\boldsymbol{T}_{mn}$ which define the directions of the corrugation axes $\boldsymbol{R_1}$ and $\boldsymbol{R_2}$ (see equation (2)). I is the average intensity of the FTR at $\theta = 0°$ normalized as described in the text.

	d8 $\boldsymbol{R}_1$	d8 $\boldsymbol{R}_2$	h8 $\boldsymbol{R}_1$	h8 $\boldsymbol{R}_2$
A/ω	0.198 ± 0.004	0.131 ± 0.002	0.204 ± 0.004	0.168 ± 0.004
ψ_0 (deg)	17.9 ± 2.0	39.8 ± 2.0	21.2 ± 2.0	-20.8 ± 2.0
Ψ_0 (deg)	-2.4 ± 2.0	19.5 ± 2.0	0.9 ± 2.0	-41.1 ± 2.0
$\boldsymbol{T}_{mn}$	$\boldsymbol{T}_{10}$	$\boldsymbol{T}_{2-1}$	$\boldsymbol{T}_{10}$	$\boldsymbol{T}_{11}$
I	1	0.34 ± 0.06	1	6 ± 2

$-70° \leqslant \theta \leqslant 70°$ for four different azimuthal angles ϕ. Figure 2 shows results for an azimuthal angle of $\phi = 5°$ at a temperature $T = 1.5$ K. First, an absorption can be seen at low fields ($*$ in figure 2). This is related to the superconducting-to-normal transition of the sample [14]; it follows the θ dependence of the upper critical field, $\mu_0 H_{c2}$, which varies approximately as $1/\cos\theta$ at such angles [10]. At high fields, quantum oscillations are observed, indicating that the sample is pure; the angular behaviour of the frequency F of the oscillations ($F \propto 1/\cos\theta$) provides a check of the angle θ [10]. At some θ, magnetic breakdown oscillations, caused by tunnelling between the Q2D and Q1D FS sections, are superimposed on the lower frequency oscillations caused by the Q2D pocket [10]. At intermediate fields there are two broad absorptions (•, ○); their (θ, ϕ) dependence (see below) [16] allows them to be unambiguously attributed to FTRs caused by the Q1D sheets.

The field positions of the FTRs were recorded for all angles studied. In order to analyse the FTRs, the experimental coordinates $\boldsymbol{B}$, θ and ϕ must be converted into the component of the field $\boldsymbol{B}_\parallel$ within the plane of the Q1D FS sheets, and the angle ψ between the normal to the sample's Q2D planes and $\boldsymbol{B}_\parallel$ (see figure 2, inset) [14]. This is done via [14] $B_\parallel = B\sqrt{\sin^2\theta\cos^2\phi + \cos^2\theta}$ and $\tan\psi = \tan\theta\cos\phi$. Each corrugation of the Q1D sheets is expected to give rise to a FTR with the ψ dependence [14, 16],

$$(\omega/B_\parallel) = A\sin(\psi - \psi_0). \tag{1}$$

Here, ω is the angular frequency of the millimetre waves, A is a constant depending on details of the FS [14], and ψ_0 defines the axis of the corrugation $\boldsymbol{R}$ (figure 2, inset). As the millimetre-wave frequency is held constant, the FTRs should lie on sinusoidal 'arches' when $1/B_\parallel$ is plotted as a function of ψ [16].

Figure 3 shows the FTR positions plotted in terms of $1/B_\parallel$ and ψ. Apart from a region close to $\psi = -40°$ where the feature associated with the superconducting-to-normal transition obscures the FTRs at some ϕ, making the exact position difficult to gauge, the data lie on two 'arches', shown as curves (figure 3); the curves were obtained by fitting the data to equation (1). This indicates that the Q1D FS of d8 κ-(BEDT-TTF)$_2$Cu(NCS)$_2$ has two distinct corrugations, with their axes $\boldsymbol{R}_1$ and $\boldsymbol{R}_2$ at angles $\psi_0 = 17.9° \pm 2.0°$ and $39.8° \pm 2.0°$ to $\boldsymbol{a}^*$ respectively.

Equivalent experiments were carried out on four samples of h8 κ-(BEDT-TTF)$_2$Cu(NCS)$_2$. (Some representative data are shown in [14].) Again, the resonance positions lie on two 'arches' (shown in figure 3), implying that the Q1D FS of h8 κ-(BEDT-TTF)$_2$Cu(NCS)$_2$ has two distinct corrugations [14]. In this case, the corrugation axes $\boldsymbol{R}_1$ and $\boldsymbol{R}_2$ are at angles $\psi_0 = 21.2° \pm 2.0°$ and $-20.8° \pm 2.0°$ to $\boldsymbol{a}^*$ respectively. The data for both materials are summarized in table 1.

κ-(BEDT-TTF)$_2$Cu(NCS)$_2$ has a monoclinic crystal structure with the crystallographic $\boldsymbol{a}$-axis at an angle of 20.3° to the normal to the Q2D planes ($\boldsymbol{a}^*$) [17]; in this respect, the crystal

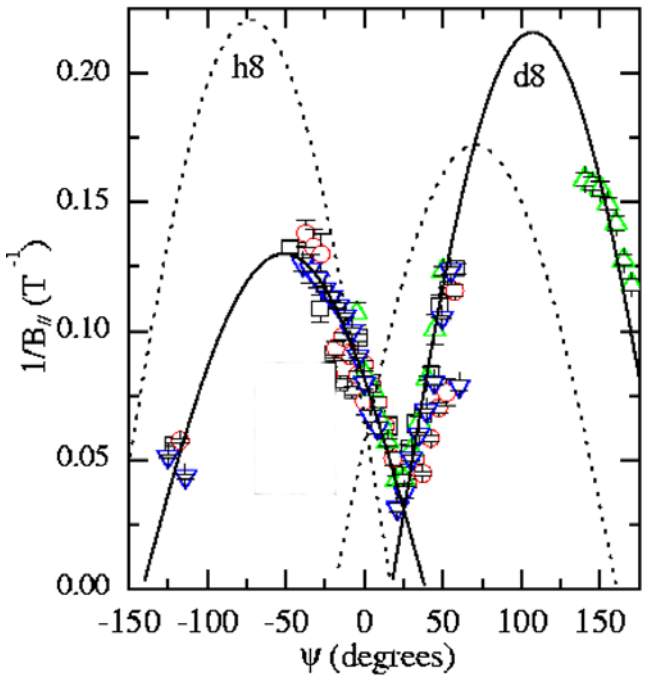

Figure 3. The field positions of the resonances in d8 κ-(BEDT-TTF)$_2$Cu(NCS)$_2$ in FTR coordinates. Data for four different ϕ ($T = 1.5$ K) are shown; squares $\phi = -40°$; circles $\phi = -25°$; upward pointing triangles $\phi = 5°$; downward pointing triangles $\phi = 35°$. Two curves ('arches'—solid curves) show the fits to the resonances using equation (1); dotted curves show equivalent fits to data from h8 κ-(BEDT-TTF)$_2$Cu(NCS)$_2$. For clarity the data points have been omitted (see [14] for representative data). Note that the larger 'arches' for h8 and d8 are a similar height, and both tend to $1/B_\parallel = 0$ at about the same value of ψ; this indicates that they are due to very similar FS corrugations. On the other hand, the smaller 'arches' for h8 and d8 are different heights and tend to $1/B_\parallel = 0$ at very different values of ψ.

structures of d8 and h8 κ-(BEDT-TTF)$_2$Cu(NCS)$_2$ appear identical [18]. Within tight-binding bandstructure, the corrugation axes of a FS usually relate to the primitive lattice translation vectors of the *real-space* lattice [19]. Rather than work in terms of the angle ψ_0, which defines the directions of the corrugation axes with respect to $\boldsymbol{a}^*$, it is more useful to use the angle Ψ_0, which relates to the real-space vector $\boldsymbol{a}$. Once this is done (table 1), it is plain that the corrugation axis $\boldsymbol{R}_1$ in both the d8 and h8 samples lies very close to the $\boldsymbol{a}$ (interlayer) direction. By contrast, the direction of $\boldsymbol{R}_2$, the second corrugation axis, differs (see caption to figure 3); with reference to the primitive lattice translation vectors

$$\boldsymbol{T}_{mn} = m\boldsymbol{a} + n\boldsymbol{c} \tag{2}$$

where m and n are integers, we find that in d8, $\boldsymbol{R}_2$ is very close in direction to $\boldsymbol{T}_{2-1}$, whereas in h8, it is close in direction to $\boldsymbol{T}_{11}$ (table 1). The reasons for the dominance of these particular directions are unclear; however, interlayer coupling through the anion layer is presently poorly understood at a molecular-orbital level. It is possible that a variety of overlap pathways may be operative and that the choice of dominant pathway through the anion layer depends very sensitively on the exact coordinates of the terminal end of the BEDT-TTF molecule [3]. In this context, it will be useful to have high-resolution structural experiments which address the detailed differences between h8 and d8 at low temperatures [18].

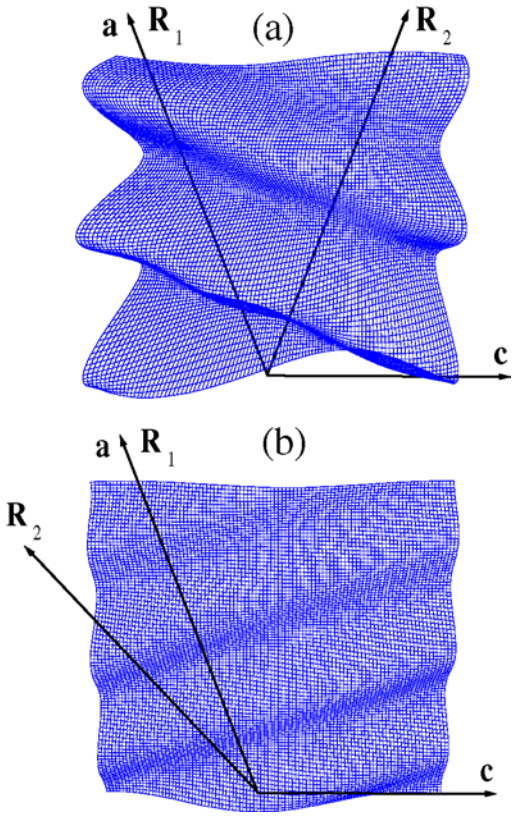

Figure 4. (a) Representation of the Q1D FS topology in h8 κ-(BEDT-TTF)$_2$Cu(NCS)$_2$ derived from the fits to the FTR data; (b) the same for d8 κ-(BEDT-TTF)$_2$Cu(NCS)$_2$ plotted at the same scale. Both are side views (i.e. looking along $\boldsymbol{k}_b$) of the Q1D sheets; corrugations have been greatly enhanced for clarity.

Finally, it is interesting to work out the relative amplitudes of the corrugations in h8 and d8 κ-(BEDT-TTF)$_2$Cu(NCS)$_2$. Models of FTR allow one to relate the intensity of the FTR to the amplitude of the FS corrugation [16]. Measurements of the dc transport properties of d8 and h8 κ-(BEDT-TTF)$_2$Cu(NCS)$_2$ suggest that the transfer integral $t_\perp$ in the $\boldsymbol{a}$ direction is similar in the two materials ($t_\perp \approx 0.04$–0.06 meV) [9]. This implies that the FS corrugations along $\boldsymbol{R}_1$ should be similar in d8 and h8 [9]; in d8 and h8 samples with equal volume the corresponding FTRs should have the same intensity [16]. The average intensities I of each FTR for $\theta = 0°$ are shown in table 1. As the samples are of different sizes, the intensities of the FTRs have been normalized to that of the FTR corresponding to $\boldsymbol{R}_1$.

Using the periodicity in k-space [17], the relative intensities of the FTRs, and the orientations Ψ_0 of $\boldsymbol{R}_1$ and $\boldsymbol{R}_2$, it is possible to make a comparison of the Q1D Fermi sheets for both materials. Figure 4 shows these representations, with the corrugations, assumed sinusoidal, shown at the same scale. This scale is chosen so that the differences between d8 and h8 are clear; in reality, the small measured value of $t_\perp$ [9] suggests that the corrugations will be on an extremely small scale.

Despite an intensive search, no features attributable to cyclotron resonance (CR) due to the Q2D FS pocket were observed in either d8 or h8, in agreement with previous studies [14].

The cavity response is dominated by the interlayer component of the sample's high-frequency conductivity [14, 15]. FS sections with more complex corrugations in the *interlayer* direction dominate the high-frequency interlayer conductivity [16]; recent measurements of κ-(BEDT-TTF)$_2$Cu(NCS)$_2$ suggest that the corrugations of the Q2D pocket are simpler and more regular than those of the Q1D sheets [9], perhaps explaining the absence of CR. Similarly, the *in-plane* corrugations of the Q1D sheet (figure 1) have little effect on the high-frequency *interlayer* conductivity (see [14–16] and references therein), and therefore do not result in detectable FTRs.

It is obvious that there is a difference between the Q1D sheets of d8 and h8, with the corrugations in h8 being stronger; the dominant corrugation has axis $\boldsymbol{R}_2$, at $-41.1°$ to $\boldsymbol{a}$. By contrast, the corrugations in d8 κ-(BEDT-TTF)$_2$Cu(NCS)$_2$ are weaker, and are dominated by that with axis $\boldsymbol{R}_1$ lying along $\boldsymbol{a}$. This suggests that the FS of d8 would be more amenable to nesting than that of h8. Our data support the importance of the 'nestability' of the Q1D sheets in κ-(BEDT-TTF)$_2$X, in agreement with other studies [2, 4, 10]. They are also in accord with the observation that the suppression of T_N and T_c (figure 1) in the κ-(BEDT-TTF)$_2$X salts with increasing pressure is predominantly caused by the uniaxial *interlayer* component of the pressure, rather than by in-plane effects [3]; uniaxial stress perpendicular to the planes is expected to increase the warping of the Fermi surface, which in turn reduces the nesting properties [3][4].

The data in this paper tend to support models for superconductivity such as those of [11, 12]. In these, the pairing of electrons is mediated by electron–electron interactions; they predict a T_c which is sensitive to the details of the FS topology. The difference between the Q1D Fermi sheets of d8 and h8 κ-(BEDT-TTF)$_2$Cu(NCS)$_2$ measured using FTR may explain the position of d8 and h8 in the phase diagram of figure 1; the Q1D Fermi sheets in the d8 samples are less corrugated (and therefore more nestable), leading to a higher T_c.

In summary, we have measured details of the FS topology of the deuterated organic superconductor κ-(BEDT-TTF)$_2$Cu(NCS)$_2$, and compared them with equivalent measurements of the undeuterated salt. We find that the Q1D FS sheets are more corrugated in the undeuterated salt, perhaps explaining the shift in T_c observed on deuteration. Our data support models for exotic d-wave superconductivity in the organics which invoke electron–electron interactions depending on the topological properties of the FS.

This work is supported by EPSRC (UK). NHMFL is supported by the US Department of Energy (DoE), the National Science Foundation and the State of Florida. Work at Argonne is sponsored by the DoE, Office of Basic Energy Sciences, Division of Materials Science under contract number W-31-109-ENG-38. We thank Stephen Hill and Stephen Blundell for constructive comments.

References

[1] Kanoda K 1997 *Physica* C **282–287** 299
McKenzie R H 1997 *Science* **278** 820
[2] Lefebvre S *et al* 2000 *Phys. Rev. Lett.* **85** 5420
[3] Müller J *et al* 2002 *Phys. Rev.* B **65** 144521
[4] Sasaki T *et al* 2002 *Phys. Rev.* B **65** 060505

[4] Given the small size of the interlayer transfer integrals in κ-(BEDT-TTF)$_2$Cu(NCS)$_2$, the strong influence of interlayer uniaxial stress on the superconductivity via increased Fermi-surface warping [3] might seem at first sight surprising. However, this idea is supported by comparisons of isostructural charge-transfer salts with different cation molecules, which give evidence that relatively small changes in the interlayer transfer integrals can lead to a radical alteration in the mechanism for superconductivity (see section 3.5 of [10] and references therein).

[5] Biggs T *et al* 2002 *J. Phys.: Condens. Matter* **14** L495
[6] Izawa K *et al* 2002 *Phys. Rev. Lett.* **88** 027002
[7] Miyagawa K *et al* 2002 *Phys. Rev. Lett.* **89** 017003
[8] Singleton J *et al* 2003 *J. Phys.: Condens. Matter* **15** L203
[9] Singleton J *et al* 2002 *Phys. Rev. Lett.* **88** 037001
Goddard P A 2003 *DPhil Thesis* University of Oxford
Goddard P A, Singleton J, Blundell S J and Schlueter J 2003 at press
[10] Singleton J and Mielke C 2002 *Contemp. Phys.* **43** 150
[11] Louati R *et al* 2000 *Phys. Rev.* B **62** 5957
[12] Kuroki K *et al* 2002 *Phys. Rev.* B **65** 100516
[13] Schlueter J A *et al* 2001 *Physica* C **351** 261
[14] Schrama J M *et al* 2001 *J. Phys.: Condens. Matter* **13** 2235
[15] Hill S 2000 *Phys. Rev.* B **62** 8699
[16] Ardavan A *et al* 1999 *Phys. Rev.* B **60** 15500
Blundell S J *et al* 1997 *Phys. Rev.* B **55** R6129
[17] Urayama H *et al* 1988 *Chem. Lett.* **1988** 463
[18] Watanabe Y *et al* 1997 *Synth. Met.* **86** 1917
[19] Ashcroft N W and Mermin N D 1976 *Solid State Physics* (Philadelphia, PA: Saunders)